

Article

Processing of Macroporous Alumina Ceramics Using Pre-Expanded Polymer Microspheres as Sacrificial Template

Marina Ciurans Oset ¹, Jan Nordin ² and Farid Akhtar ^{1,*}

¹ Division of Materials Science, Luleå University of Technology, 971 87 Luleå, Sweden; marciu-5@student.ltu.se

² Akzo Nobel Pulp and Performance Chemicals AB, Expancel, P.O. Box 13000, SE-850 13 Sundsvall, Sweden; jan.nordin3@nouryon.com

* Correspondence: farid.akhtar@ltu.se

Received: 17 October 2018; Accepted: 2 November 2018; Published: 6 November 2018



Abstract: Shaped porous ceramics have proven to be the most adapted materials for several industrial applications, both at low and high temperatures. Recent research has been focused on developing shaping techniques, allowing for a better control over the total porosity and the pores characteristics. In this study, macroporous alumina foams were fabricated by gel-casting using pre-expanded polymeric microspheres with average sizes of 40 μm , 20 μm , and 12 μm as sacrificial templates. The gel-casting method, as well as the drying, debinding, and presintering conditions were investigated and optimized to process mechanically strong and highly porous alumina scaffolds. Furthermore, a reliable model relating the amount of pre-expanded polymeric microspheres and the total porosity of the presintered foams was developed and validated by mercury intrusion porosimetry measurements. The electron microscopy investigation of the presintered foams revealed that the size distribution and the shape of the pores could be tailored by controlling the particle size distribution and the shape of the wet pre-expanded microspheres. Highly uniform and mechanically stable alumina foams with bimodal porosity ranging from 65.7 to 80.2 vol. % were processed, achieving compressive strengths from 3.3 MPa to 43.6 MPa. Given the relatively open pore structure, the pore size distribution, the presintered mechanical strength, and the high porosity achieved, the produced alumina foams could potentially be used as support structures for separation, catalytic, and filtration applications.

Keywords: gel-casting; sacrificial templating; macroporous alumina; pre-expanded polymeric microspheres

1. Introduction

Several industrial applications, such as water filters [1], catalyst supports for hot gas filtration [2,3], molten metal filters [4], thermal insulators [5], and bio-compatible scaffolds [6] require the properties offered by shaped ceramic materials with controlled porosity. Each of these particular applications have requirements regarding the pore size distribution, the volume fraction of porosity, the fraction of open porosity, and the degree of connectivity [7]. For instance, filtration and biomedical applications usually require macropores and high pore space accessibility, while mesopores and closed porosity are preferred for thermal insulation purposes. In general, the porosity has a strong influence on physical and mechanical properties such as the thermal conductivity [8], the fluid and gas permeability [9], and the mechanical strength [10]. Therefore, the processing of porous ceramics foams with tailored porosity is of interest.

A wide variety of techniques have been reported as suitable for the production of hierarchically structured porous ceramics. These are usually classified in three main processing strategies: replication, direct foaming, and sacrificial templating [11]. Replication [12] consists of impregnating or infiltrating a template with highly dispersed ceramic suspensions. Upon sintering, the template is removed and a positive replica of it is obtained. Ceramic foams with high porosity and highly open pore space could be obtained in replication method. In direct foaming [13] air bubbles are incorporated into highly loaded slurries, either by mechanical frothing or direct gas injection. Alternatively, multiple direct foaming techniques based on the emulsification of a polymer phase within a ceramic powder suspension have been recently developed [14–16]. Reticulated ceramics with moderate to high porosity and partially open pore space have also been obtained. Both colloidal particles [17] and surfactants [18] have been reported as effective foam and emulsion stabilizers to prevent the coarsening of the microstructure due to coalescence. In sacrificial templating [11], a sacrificial disperse phase is incorporated into highly loaded ceramic slurries. After complete drying of the ceramic foams, the template is removed and pores representing a negative replica of the original templating phase are left behind. Multiple techniques are included in this processing strategy. For instance, freeze casting [19] uses the solvent of highly dispersed slurries as templating phase.

Gel-casting is a colloidal near-net shape forming technique that was developed in the early 1990s that can be easily combined with sacrificial templating to process highly tailored porous ceramics [20]. It comprises the casting of highly-loaded suspensions containing ceramic powder and organic additives such as binders and dispersants (typically around 3–4 wt. %). The gelation of the binder in the slurry is induced by either thermal or chemical means, which results in the formation of a hydrophilic cross-linked polymeric network. The gel holds the ceramic particles together during the drying and organics burn-out prior to the sintering of green bodies [21,22]. Gel-cast ceramic bodies are characterized by relatively high green mechanical strengths, low debinding shrinkages, and highly homogeneous microstructures with small or no defects [23]. Several materials, both natural and synthetic, have been reported in literature as suitable sacrificial templates. For instance, Qian et al. [24] used fly ash cenospheres (FAC) in the gel-casting of macroporous mullite. FAC are usually formed during the combustion of mineral coal, and their particle size distribution and morphology can be controlled by tuning the coal composition and the cooling conditions. Consequently, the size distribution and the morphology of the pores can be directly controlled. Nevertheless, the addition of FAC was observed to mainly contribute to the formation of closed pores, resulting in ceramic foams with significantly low permeabilities [24].

Dash et al. [25] used naphthalene particles in the gel-casting of macroporous hydroxyapatite scaffolds. It was found that these particles increased both the total porosity and the connectivity between individual pores. However, the agglomeration of naphthalene particles at higher contents resulted in the interdependency between the total porosity and the pore size distribution. Furthermore, the difficulty to predict the morphology of these aggregates resulted in a lack of control over the final shape and size of the pores. Wan et al. [26] used glutinous rice flour (GRF) in the manufacturing of mesoporous silica. The GRF content determined the total porosity of the foams. However, GRF is mainly composed of starch, which swells as it absorbs hot water. The risk of cracking during the drying process is thus significant, and neither the morphology nor the size distribution of the pores can be controlled.

A promising alternative to the pore-forming agents mentioned above is the use of expandable polymeric microspheres, which consist of a thermoplastic shell encapsulating an appropriate blowing agent. These microspheres are obtained in the unexpanded state, but their expansion can be easily induced by heating them to temperatures close to the glass transition temperature of the thermoplastic shell. For instance, Andersson et al. [27] used unexpanded thermoplastic microspheres in the gel-casting of macroporous alumina. With the processing method developed by the authors, the thermal gelation of the binder induced the softening of the polymeric shell and resulted in subsequent expansion of the microspheres. Highly homogeneous foams with almost spherical pores,

a high fraction of open porosity and a relatively high permeability were obtained. Nevertheless, the expansion of the microspheres cannot be fully controlled and can limit the control over the final pore size distribution and the total porosity of the foams.

In the present study, the viability of wet pre-expanded polymeric microspheres as sacrificial templates for shaping porous alumina ceramics is assessed. These microspheres are dispersed in water and expanded prior to the processing of the ceramic foams. As a result, they do not expand during the gel-casting process, enabling a stricter control over the pore size distribution and the total porosity of the sintered foams. Furthermore, small mass of expanded microspheres are required to process ceramic foams with high volume fraction of porosity. In this work, a suitable fabrication method based on gel-casting and sacrificial-templating has been developed and optimized. Particular attention has been given to the dispersion of the microspheres within the suspension and degassing of entrapped air bubbles. The mass loss and the shrinkage of the specimens throughout the drying process, the thermal behavior of the green bodies, as well as the mechanical strength, the density, the porosity, and the pore structure of presintered alumina ceramics have been investigated.

2. Materials and Methods

2.1. Materials

Two different commercially available α -alumina powders were used: A-16 SG (Alcoa, Blount County, TN, USA), with an average particle size of 0.4 μm and specific surface area of 9.0 m^2/g , and AKP-15 (Sumitomo Chemical Co., Ltd., Tokyo, Japan), with an average particle size of 0.6 μm and specific surface area of 3.5 m^2/g . A 25 vol. % aqueous solution of polyacrylic acid (PAA, Polysciences, Inc., Warrington, PA, USA) with $M_W = 50,000$ g/mol was used as a dispersing agent. Alternatively, sodium dodecyl sulfate (SDS, Sigma-Aldrich Chemie GmbH, Darmstadt, Germany) with $M_W = 288.38$ g/mol was also used as a dispersing agent. The amount of SDS or PAA added to the slurry was equal to 1 wt. % with respect to the alumina powder. Regarding the acrylic binder, methyl methacrylate (MMA, Sigma-Aldrich Chemie GmbH, Darmstadt, Germany) with $M_W = 100.12$ g/mol, and *N,N'*-methylenebisacrylamide (MBAM, Sigma-Aldrich Chemie GmbH, Darmstadt, Germany) with $M_W = 154.17$ g/mol were used as monomer and cross-linker, respectively. The total amount of binder corresponded to 4 wt. % of the total alumina, and the monomer to cross-linker weight ratio was set to 5:1. Ammonium persulfate (APS, Sigma-Aldrich Chemie GmbH, Darmstadt, Germany) with $M_W = 228.20$ g/mol was used as a free radical initiator. The amount of APS added to the slurry was equal to 0.5 wt. % with respect to the monomer. 1-butanol (Merck Millipore, Darmstadt, Germany) was used as an anti-foaming agent. Finally, tetramethylethylenediamine (TEMED, Sigma-Aldrich Chemie GmbH, Germany) with $M_W = 116.20$ g/mol was used as a catalyst. The total amount of TEMED added to the slurry corresponded to 20 wt. % with respect to the monomer. Three different types of Expancel[®] wet-expanded microspheres (Akzo Nobel Pulp and Performance Chemicals AB, Sundsvall, Sweden) were used as sacrificial templates (Figure 1). The product density and the solid content of each Expancel[®] type were provided by Akzo Nobel Pulp and Performance Chemicals AB (Table 1). The volume of dried microspheres per unit mass of wet product, v , was determined with Equation (1):

$$v = \frac{\text{wt. \% solid content}}{\rho_{\text{product}}} \quad (1)$$

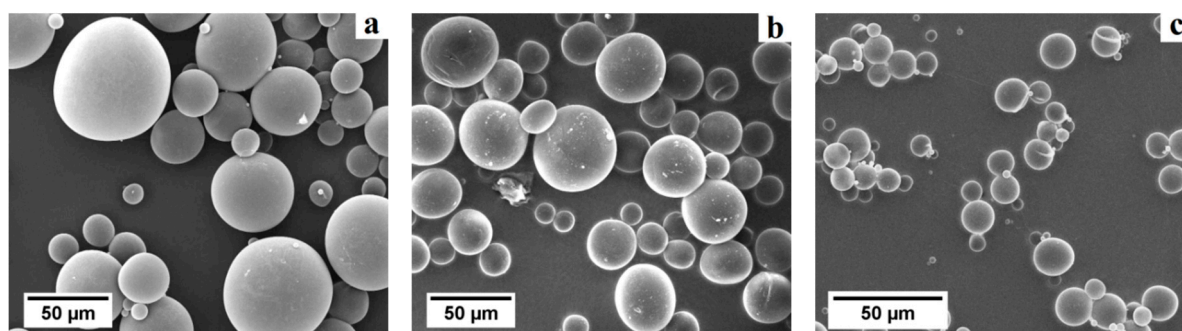


Figure 1. Scanning electron microscopy (SEM) micrographs of the three types of wet expanded Expancel[®] microspheres used in this study: (a) WE 40 µm, (b) WE 20 µm, and (c) WE 12 µm.

Table 1. Properties of the polymer microspheres (WE: wet expanded) used in this study, as provided by Akzo Nobel Pulp and Performance Chemicals AB. Volume of dried microspheres per unit mass of wet product (v) determined using Equation (1). Morphological characterization by SEM image analysis: determination of the mean particle size over volume and the mean aspect ratio.

| Expancel [®] Grade | Product Density (g/cm ³) | Solid Content (wt. %) | v (cm ³ /g) | Mean Particle Size (µm) | Mean Aspect Ratio |
|-----------------------------|--------------------------------------|-----------------------|--------------------------|-------------------------|-------------------|
| WE 40 µm | 0.024 | 17.2 | 7.167 | 45.3 | 0.95 |
| WE 20 µm | 0.030 | 24.4 | 8.133 | 38.5 | 0.94 |
| WE 12 µm | 0.060 | 16.0 | 2.667 | 14.0 | 0.97 |

2.2. Specimen Preparation

Figure 2 shows the flowchart of the gel-casting process used in this study to prepare the ceramic specimens. First, a water-based organic premix containing the monomer (MMA) and the cross-linker (MBAM) was prepared. After 30 min of mixing at room temperature, the dispersing agent (either PAA or SDS) was added and mixed for 5 min. Next, half of the total alumina powder was slowly added to the organic premix in order to prevent the formation of agglomerates. The anti-foaming agent (1-butanol) was then added, followed by the remaining ceramic powder. The resulting slurry was transferred to a high-density polyethylene bottle already containing zirconia milling balls. The weight ratio between the zirconia balls and the alumina powder was 1:1. After milling at high speed for 24 h, the ceramic slurry was filtered to remove the milling balls. The initiator (APS) and a water-based dispersion containing the appropriate amount of Expancel[®] microspheres were then added, and the ceramic slurry was homogenized by magnetic stirring for 30 min at room temperature. After ultrasonic degassing, the catalyst (TEMED) was added and the slurry was mixed for 30 s before casting. In this study, commercially available truncated cone shaped rubber molds were used. The dimensions of the upper and lower diameters were 70 mm and 45 mm, respectively, while the height was 35 mm. Depending on the batch, the molds were filled up to a height of 17 to 27 mm, in order to allow the casting of three specimens of equal dimensions. The molds were not covered after casting, so that the upper surface of the cast bodies was in contact with the air throughout the whole process.

After 6 h of gelation at room condition, the specimens were dried in a furnace to better control both the temperature and the relative humidity during the process. Based on the drying conditions proposed by Andersson et al. [27], the temperature was increased stepwise from 25 °C to 50 °C over a time period of 71 h, at a relative humidity of $75 \pm 5\%$. Next, the specimens were heated at 100 °C for 1 h, thus completing a total drying time of 72 h (three days). This stage was carried out at a relative humidity of $25 \pm 5\%$ to maximize the removal of water. After complete drying, the green bodies were unmolded and underwent organics burn-out and presintering process in air. The burn-out step consisted of 3 h at 600 °C, while presintering was performed at 1200 °C during 2 h with a heating rate of 5 °C/min. Finally, the cooling of the specimens took place in the furnace to minimize the risk of cracking due to thermal shock.

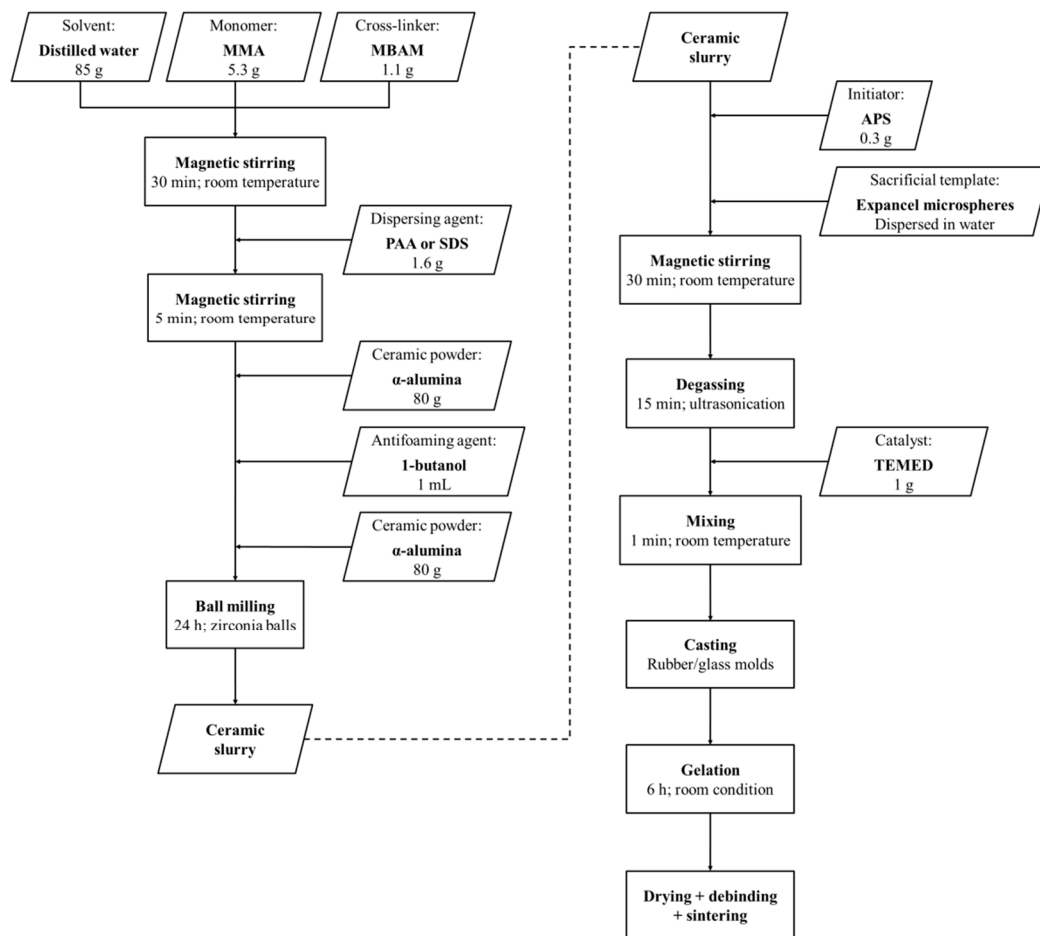


Figure 2. Flowchart of the gel-casting and sacrificial templating procedure followed in the present study to prepare the macroporous alumina specimens.

2.3. Characterization

The bulk density and the pore size distribution of the presintered foams were determined by mercury intrusion porosimetry with a Micromeritics AutoPore III 9410 (Micromeritics, Aachen, Germany). The considered pore size interval was 30 nm to 125 μm . The surface tension and the contact angle of the mercury were assumed to be 0.485 N/m and 130°, respectively. The total vol. % porosity was then analytically determined using Equation (2), where ρ_{bulk} , ρ_{alumina} and ρ_{air} represent the bulk, the skeletal and the air densities, respectively ($\rho_{\text{air}} = 0.012 \text{ g/cm}^3$).

$$\text{vol. \% porosity} = \frac{\rho_{\text{alumina}} - \rho_{\text{bulk}}}{\rho_{\text{alumina}} - \rho_{\text{air}}} \quad (2)$$

To evaluate the mechanical properties of presintered foams, three cubic samples with sides of 10 mm were cut from each specimen and carefully polished until two highly parallel and smooth surfaces were obtained. Their compressive strength was then measured with an Instron 5967 (Instron, Norwood, MA, USA) testing machine, using a 2 kN load cell and a crosshead speed of 0.5 mm/min. The thermal behavior of the green bodies was studied simultaneously by differential scanning calorimetry (DSC) and thermogravimetric analysis (TGA) with a STA 449 F3 Jupiter® (NETZSCH, Gerätebau GmbH, Germany). Argon was used as protective gas and air as purge gas. Two alumina crucibles were used, one containing the sample and one empty as reference. Scanning electron microscopy (SEM) was used to investigate the Expancel® microspheres and the microstructure of the ceramic foams. The observations were performed with a JEOL NeoScope JCM-6000 Plus (JEOL USA,

Inc., Peabody, MA, USA) under high vacuum and high acceleration voltage (15 kV). The micrographs thus obtained were quantitatively studied by image analysis using the software *ImageJ*.

To monitor the mass loss and the shrinkage of the alumina foams, the mass and the upper diameter of the specimens were periodically measured during the drying process with a high precision balance and measuring tape, respectively. As already mentioned, the upper surface of the cast bodies was left free, while all other surfaces were in contact with the mold throughout the drying process. It was thus decided to investigate the drying shrinkage on the upper surface, since the dimensional variation due to water evaporation was expected to be significantly higher on this surface than in any other. The cumulative mass loss and radial shrinkage were determined with Equations (3) and (4), respectively, where m_0 and D_0 represent the mass and the upper diameter after gelation, and m_i and D_i correspond to the mass and the upper diameter of the specimen after the step.

$$\% \text{ mass loss} = \frac{m_0 - m_i}{m_0} \times 100 \quad (3)$$

$$\% \varepsilon_r = \frac{D_0 - D_i}{D_0} \times 100 \quad (4)$$

3. Results and Discussion

The processing of porous alumina ceramics using pre-expanded polymer spheres as sacrificial template can offer a close control over the porosity and pore size distribution. To achieve a well-tailored porous structure, the entrapment of air bubbles in the suspension containing alumina and pre-expanded polymer spheres needs to be minimized. Indeed, neither the size nor the shape of these air bubbles can be directly controlled, which results in a significant fraction of non-controlled porosity in the final alumina foams. Given their relatively large size, these air bubbles are highly detrimental for the mechanical properties of the foams. The influence of dispersant on the entrapment of non-controlled air bubbles within the slurry is shown in Figure 3. The use of the ionic surfactant sodium dodecyl sulfate as dispersing agent was observed to increase the heterogeneity of the microstructure due to the presence of air bubbles in the ceramic suspension. As a result, alumina foams containing non-controlled macropores, in addition to the macropores generated by the pre-expanded microspheres, and cracks were obtained (Figure 3a). On the other hand, significantly lower amounts of air bubbles were entrained into the slurries when using polyacrylic acid (PAA), a water soluble ionic polyelectrolyte, and were effectively removed by ultrasonic degassing (Figure 3b). As can be seen in Table 2, the non-controlled porosity could be reduced to as low as 5.1 vol. % in foams prepared with high volume fraction of microspheres with 15 min of ultrasonic degassing. In foams prepared with low volume fraction of microspheres, the non-controlled porosity could only be reduced to 11.6 vol. % after the same degassing time. Thus, the addition of PAA as dispersing agent, combined with ultrasonic degassing of the slurry, is required to produce macroporous alumina ceramics using pre-expanded polymeric microspheres as sacrificial template.

Table 2. Type of alumina and microsphere used as template, solid loading, targeted porosity, and degassing time for all ceramic slurries prepared in this study. Bulk density and total porosity of the corresponding presintered alumina foams.

| Batch No. | Alumina Type | Expancel®Grade | Total Solid Loading (wt. %) | Dried Microspheres (wt. %) | Targeted Porosity (vol. %) | Degassing Time (min) | Bulk Density (g/cm ³) | Total Porosity (vol. %) |
|-----------|--------------|----------------|-----------------------------|----------------------------|----------------------------|----------------------|-----------------------------------|-------------------------|
| 1 | AKP-15 | WE 40 μm | 60.5 | 0.89 | 70.0 | 15 | 0.94 | 75.1 |
| 2 | AKP-15 | WE 40 μm | 61.8 | 0.40 | 50.0 | 10 | 1.26 | 66.7 |
| 3 | A-16 SG | WE 20 μm | 54.8 | 1.08 | 70.0 | 15 | 0.91 | 76.0 |
| 4 | AKP-15 | WE 20 μm | 59.8 | 0.47 | 50.0 | 15 | 1.45 | 61.6 |
| 5 | A-16 SG | WE 12 μm | 53.2 | 1.91 | 70.0 | 10 | 0.75 | 80.2 |
| 6 | A-16 SG | WE 12 μm | 56.0 | 0.88 | 50.0 | 10 | 1.29 | 65.7 |

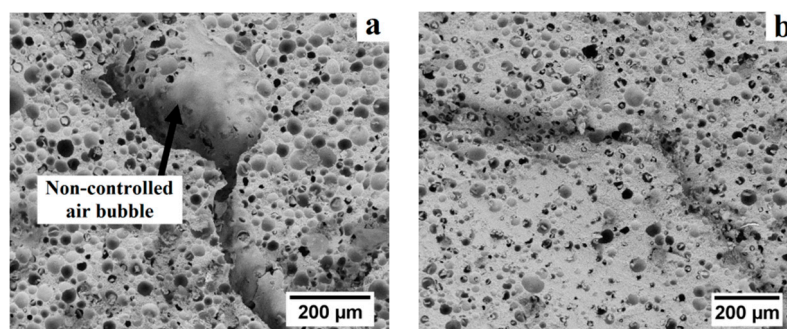


Figure 3. Presintered alumina foams prepared using different dispersing agents: (a) sodium dodecyl sulfate (SDS), an anionic surfactant and (b) polyacrylic acid (PAA), a water-soluble anionic polyelectrolyte.

The microstructural uniformity and integrity of gel-cast ceramic foams are dependent on the gelation method [21,22]. Both thermal and catalytic gelation of suspensions of alumina and pre-expanded polymer microspheres were thus investigated. In the case of thermal gelation, most acrylic binders require the slurries to be heated to a temperature of 75–80 °C, which is in the expansion window for the thermoplastic microspheres [27]. In our case, the gelation temperature caused the collapse of pre-expanded microspheres over time and resulted in the formation of loose ceramic shells trapped in the pores upon presintering (Figure 4a). The thermal gelation of as-cast bodies resulted in the contamination of pores. The use of a catalyst (TEMED) enabling the gelation of the binder without additional heating was then envisaged, which resulted in a homogeneous and contamination-free microstructure (Figure 4b).

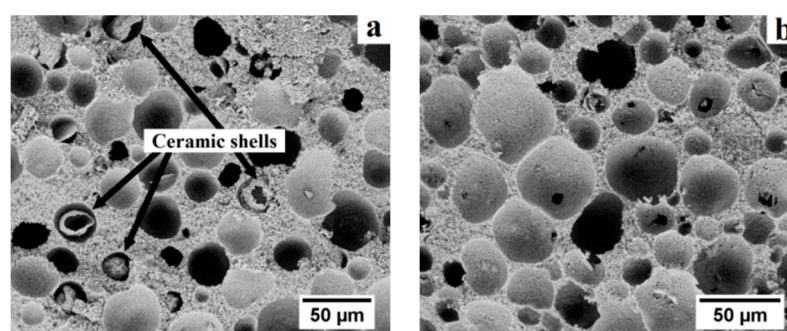


Figure 4. Fracture surface of presintered alumina foams prepared using different gelation methods: (a) thermal gelation and (b) catalytic gelation.

The gel-cast green bodies contain approximately the same amount of solvent as the corresponding initial slurries. Therefore, the drying of green bodies is of significance to minimize the dimensional distortion and the cracking. The evolution of both the mass loss and the radial shrinkage of the gel-cast alumina foams were monitored throughout the drying process (Figure 5a,b, respectively). It can be seen in Figure 5 that the first 48 h of drying are characterized by a high mass loss rate, related to the evaporation of the water adsorbed to the external surfaces. This first drying stage, carried out at a relative humidity of $75 \pm 5\%$, consisted of 24 h at 25 °C followed by 24 h at 35 °C. With the increase in liquid-gas interface upon drying, the ceramic particles come closer and eventually into contact with each other. At macroscale, the drying mechanism results in a relatively rapid shrinkage of the green bodies. The last 24 h of drying, carried out at a relative humidity of $25 \pm 5\%$, and consisting of 23 h at 50 °C followed by 1 h at 100 °C, show relatively low mass loss and shrinkage rates, corresponding to the removal of entrapped water through open porosity.

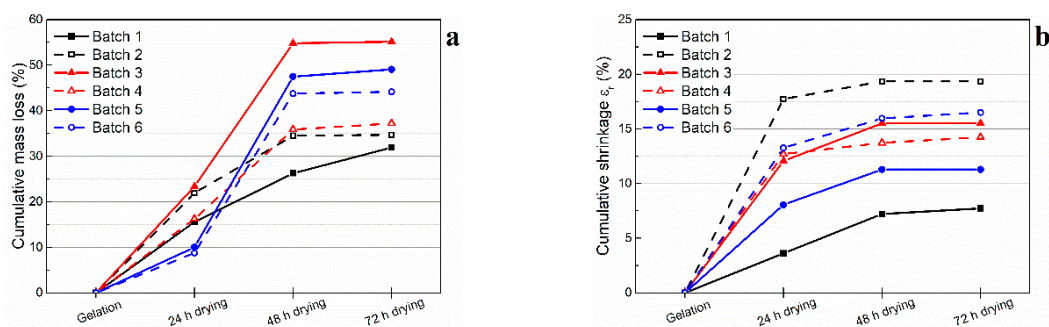


Figure 5. Effect of the drying conditions on (a) cumulative mass loss and (b) cumulative radial shrinkage. The composition and properties of batches 1 to 6 are summarized in Table 2.

The suspensions with high total solid loadings were observed to result in low mass losses. However, no clear correlation between the amount of polymeric microspheres in the slurry and the mass loss upon drying could be identified. A small fraction of dried microspheres (0.5 to 1.9 wt. %) were required to achieve 61.6 to 80.2 vol. % porosity, respectively. It was thus concluded that the amount of solvent was the influencing parameter on the evolution of the mass loss, while the moisture added to the slurry by the wet microspheres had no significant effect. Regarding the shrinkage of the green ceramic foams, the amount of pre-expanded microspheres in the slurry was found to have a major influence. Higher shrinkage was observed in moderate porosity foams (61.6 to 66.6 vol. %) with large and isolated pores, prepared with small volume fraction of polymer microspheres. On the other hand, high porosity foams (75.1 to 80.2 vol. %) with closely packed pores, prepared with larger volume fraction of microspheres, exhibited lower shrinkages. The drying shrinkage was observed to be rather homogeneous and no cracking occurred in the dried foams with a total solid loading higher than 53.2 wt. %, corresponding to a porosity of 80.2 vol. %. It is thus expected that crack-free presintered alumina foams with porosity higher than 80 vol. % could be obtained from slurries containing total solid loadings of 60 wt. % and higher.

After drying, the gel-cast green bodies underwent organics burn-out and presintering to achieve accessible pore space and sufficient mechanical stability. Figure 6a shows the DSC and TGA curves of a 66.7 vol. % porosity alumina foam produced with WE 40 μm microspheres. In this particular specimen, organic additives represented 3.5 wt. %. The thermal degradation of the gelled binder and the expandable microspheres was particularly critical, as these are the most abundant organic additives in the dried specimens. Two main thermal events can be observed on the TGA curve presented in Figure 6b. The first one, at approximately 260 $^{\circ}\text{C}$, is related to the degradation of the PMMA polymeric network. According to the literature, the decomposition of this compound takes place between 240 $^{\circ}\text{C}$ and 360 $^{\circ}\text{C}$ [28]. The second event is observed in the range 320–400 $^{\circ}\text{C}$ and can be related to the degradation of the polymeric microspheres, as the thermal decomposition of acrylonitrile is reported to occur at around 410 $^{\circ}\text{C}$ [29]. No significant variation in the mass of the specimens was observed after 600 $^{\circ}\text{C}$. All the slurries prepared in this study contained as low as 3.5 to 5 wt. % in organic additives, including the thermoplastic microspheres. Given these low concentrations and the reported degradation temperatures for the remaining additives [30–32], a fast organics burn-out step with a heating rate of 5 $^{\circ}\text{C}/\text{min}$ was proven effective in removing all the organic additives without compromising the structural integrity of the scaffolds. Indeed, no cracks were observed to appear during the organics burn-out and presintering process.

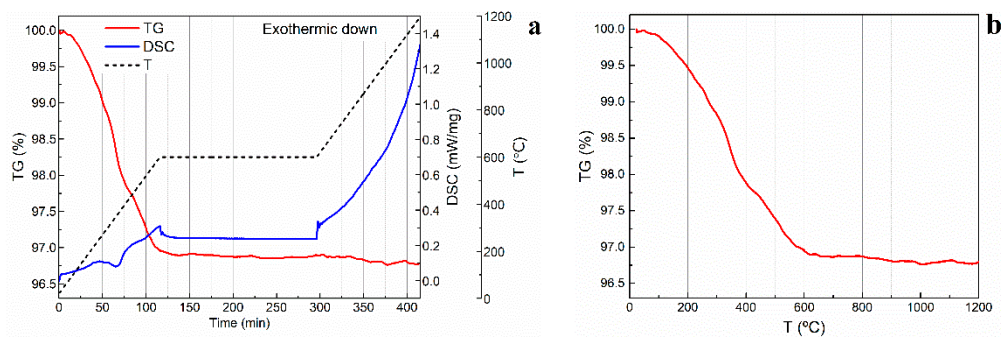


Figure 6. Thermal analysis of a high porosity (66.7 vol. %) alumina foam produced with WE 40 μm microspheres: (a) differential scanning calorimetry (DSC) and thermogravimetric analysis (TGA) curves as a function of time and (b) TGA curve as a function of temperature.

The addition of pre-expanded polymer microspheres as sacrificial templates to ceramic powder systems can simultaneously control the total porosity, the pore size distribution, and the morphology of pores in the ceramic foams. The total porosity is mainly determined by the amount of microspheres added to the ceramic slurries. The total volume of microspheres ($V_{\text{microspheres}}$) required to achieve a certain level of porosity (vol. % porosity) was determined with Equation (5), where m_{alumina} corresponds to the total mass of alumina powder in the slurry and ρ_{skeletal} represents the density of the ceramic struts after presintering. The mercury intrusion porosimetry (MIP) measurements carried out in the present study revealed that alumina scaffolds presintered at 1200 $^{\circ}\text{C}$ for 2 h exhibited strut densities of $3.7 \pm 0.2 \text{ g/cm}^3$. Therefore, ρ_{skeletal} in Equation (5) was taken to be 95% the density of dense alumina. The mass of wet product was then determined from $V_{\text{microspheres}}$ and the volume of dried microspheres per unit mass of each wet product. The differences between the target porosity and the total porosity measured by MIP arise due to the volume fraction of entrapped air bubbles.

$$V_{\text{microspheres}} = \frac{\text{vol. \% porosity}}{(1 - \text{vol. \% porosity})} \times \frac{m_{\text{alumina}}}{\rho_{\text{skeletal}}} \quad (5)$$

Cellular alumina foams produced in this study exhibited a hierarchical pore structure, as shown in Figure 7. For instance, Figure 7a–c show low magnification micrographs of the fracture surface of presintered high porosity alumina scaffolds produced with different types of microspheres. A highly uniform microstructure can be observed, with well-dispersed primary macropores interconnected by secondary pores. No evident microcracks, voids or ceramic particles agglomerates are observed. Figure 7d shows a higher magnification micrograph of the presintered ceramic struts, where the third level of porosity (i.e., inter-particle pores between alumina particles) can be observed. These tertiary pores are expected to decrease in size and eventually disappear upon sintering at high temperature.

The particle size distribution in number (Figure 8a–c) and the aspect ratio of the primary macropores were investigated by image analysis of SEM micrographs using the software *ImageJ* (Table 1). WE 40 μm microspheres were found to exhibit sizes in the range 20 to 50 μm , WE 20 μm microspheres in the range 5 to 40 μm , and WE 12 μm microspheres in the range 2 to 16 μm (occurrence over 5%). This same method was used to determine the size distribution in number and the morphology of the primary macropores in presintered foams (Table 3). A correction factor of $2/\sqrt{3}$ was used to determine the actual pore size, as proposed by Naranda et al. [33]. Due to random sectioning during the sample preparation for SEM imaging, pores look smaller on the micrographs than the original pore size. All specimens prepared with WE 40 μm and WE 12 μm microspheres exhibited bimodal pore size distributions with highly overlapped modes (e.g., Figure 8d,f), while those prepared with WE 20 μm were characterized by a monodispersed pore size distribution (e.g., Figure 8e).

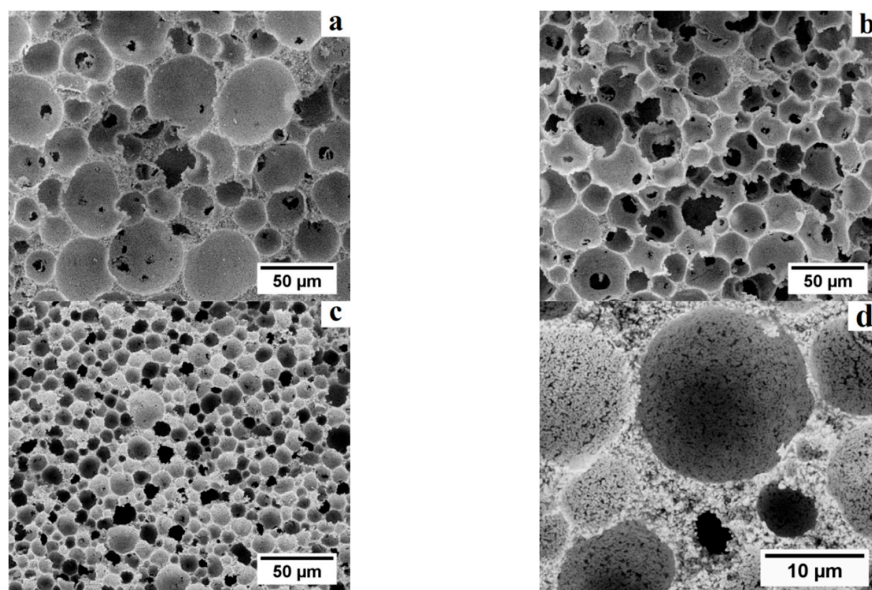


Figure 7. Fracture surface of presintered alumina foams: low magnification SEM micrographs of (a) 75.1 vol. % porosity foam produced with WE 40 μm , (b) 76.0 vol. % porosity foam produced with WE 20 μm and (c) 80.2 vol. % porosity foam produced with WE 12 μm ; (d) high magnification SEM micrograph of a 65.7 vol. % porosity foam produced with WE 12 μm .

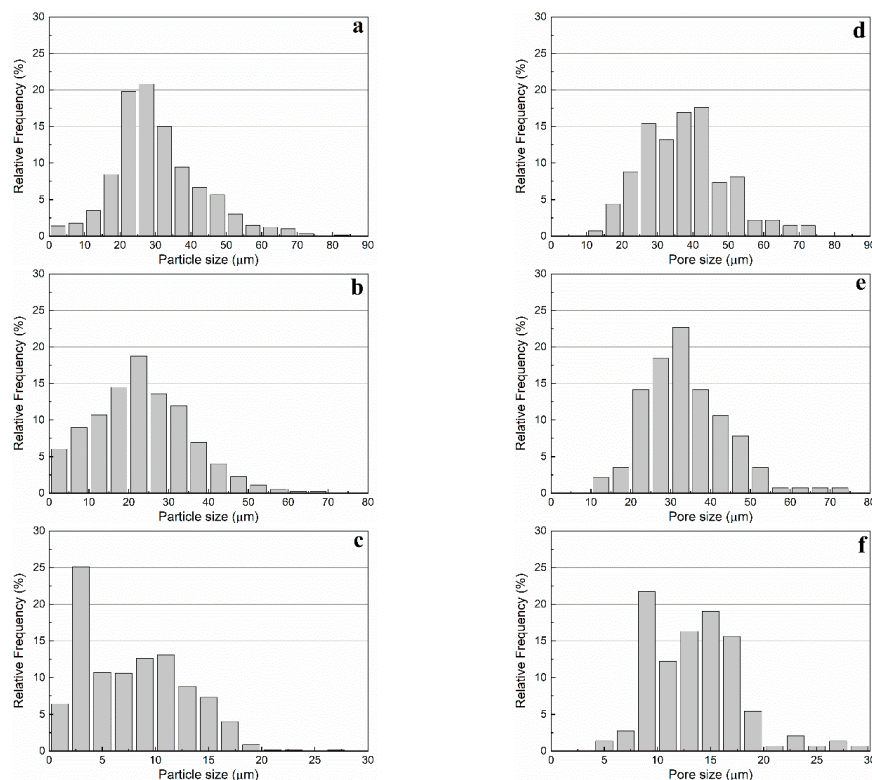


Figure 8. Particle size distribution by number of the three types of wet pre-expanded microspheres used in this study: (a) WE 40 μm , (b) WE 20 μm , and (c) WE 12 μm . Primary macropore size distribution by number of presintered porous alumina foams: (d) 75.1 vol. % porosity foam produced with WE 40 μm , (e) 76.0 vol. % porosity foam produced with WE 20 μm and (f) 80.2 vol. % porosity foam produced with WE 12 μm .

Table 3. Morphological characterization of pores: mean size over volume and mean shape factor of the primary macropores generated by the sacrificial template, as well as mean secondary interconnecting pore and mean tertiary inter-particle pore sizes (as determined by mercury intrusion porosimetry) and degree of openness of the pore structure. Compressive strength of the presintered alumina foams.

| Batch No | Mean Primary Macropore (μm) | Mean Aspect Ratio | Mean Inter-Connecting Pore (μm) | Mean Inter-Particle Pore (μm) | Degree of Openness (%) | Compressive Strength (MPa) |
|----------|--|-------------------|--|--|------------------------|----------------------------|
| 1 | 42.6 | 0.95 | 4.07 | 0.24 | 9.6 | 10.2 \pm 0.6 |
| 2 | 41.1 | 0.96 | 2.18 | 0.30 | 5.3 | 24.1 \pm 1.0 |
| 3 | 38.3 | 0.95 | 6.63 | 0.13 | 17.3 | 3.4 \pm 0.1 |
| 4 | 34.2 | 0.93 | 2.19 | 0.29 | 6.4 | 38.3 \pm 1.6 |
| 5 | 15.4 | 0.96 | 1.43 | 0.15 | 9.3 | 7.7 \pm 0.5 |
| 6 | 13.2 | 0.96 | - | 0.23 | - | 40.0 \pm 3.6 |

Overall, the mean primary macropore size did not differ more than 11% with respect to the mean particle size of the corresponding pre-expanded microsphere grade. All presintered alumina foams produced in this study exhibited a partially open cellular microstructure. Specimens prepared with WE 40 μm microspheres had primary macropores of sizes ranging from 25 to 55 μm (occurrence over 5%). Furthermore, specimens prepared with WE 20 μm microspheres had primary macropores in the range 25 to 50 μm , while those prepared with WE 12 μm microspheres exhibited primary macropores in the range 10 to 20 μm (occurrence over 5%). Besides sacrificial-templating, such cellular macroporous ceramics are usually produced by direct foaming techniques. For instance, Barg et al. [18] prepared cellular alumina foams with macropores ranging from 0.5 to 3 mm, while alumina scaffolds developed by Gonzenbach [17] exhibited primary macropores ranging from 10 to 300 μm . Ceramic scaffolds processed by traditional foaming techniques usually exhibit wide pore size distributions with significantly large pores. The materials and methods described in the present study allow the processing of macroporous ceramics with significantly narrower pore size distributions and small pore sizes. In particular, given their relatively high specificity and their small mean pore size, foams prepared with WE 12 μm microspheres could potentially be used as diesel particulate filters (DPFs) [34].

Regarding the shape distortion, the mean aspect ratio of the pores did not differ more than 1% with respect to the corresponding microsphere grade (Table 3). It was thus concluded that microspheres are not irreversibly deformed during the mixing of the slurry, and so the shape of the pores is completely determined by the shape of the wet pre-expanded microspheres.

Secondary interconnecting pores and tertiary inter-particle pores are critical for the mechanical and the transport properties of ceramic foams. However, these could not be characterized by image analysis of SEM micrographs. Therefore, the pore size distribution of presintered foams was investigated by mercury intrusion porosimetry (Figure 9). For all specimens analyzed, a relatively narrow peak was observed in the range 0.13–0.30 μm , corresponding to the tertiary inter-particle pores between alumina particles. In general, a second lower peak could also be identified in the range 1.43–6.63 μm , corresponding to the secondary interconnecting pores. This second peak was generally more pronounced in foams with 75.1 to 80.2 vol. % porosity (e.g., Figure 9a) than in foams with 61.6 to 66.7 vol. % porosity (e.g., Figure 9b). The close-packing of the microspheres in specimens with high volume fraction of porosity results in relatively large windows connecting individual pores after the organics burn-out. In mercury intrusion porosimetry, all pores are assumed to be cylindrical. Consequently, these results must be interpreted as the size of the largest access to the open pores and not the actual size of the inner pores. The degree of openness of the presintered alumina scaffolds was determined as the ratio of mean size of secondary interconnecting pores to mean size of macropores on a volume basis, as proposed by Pulko et al. [35] (Table 3). It was thus concluded that porous alumina foams with a significantly open pore space can be produced using pre-expanded thermoplastic microspheres as sacrificial templates.

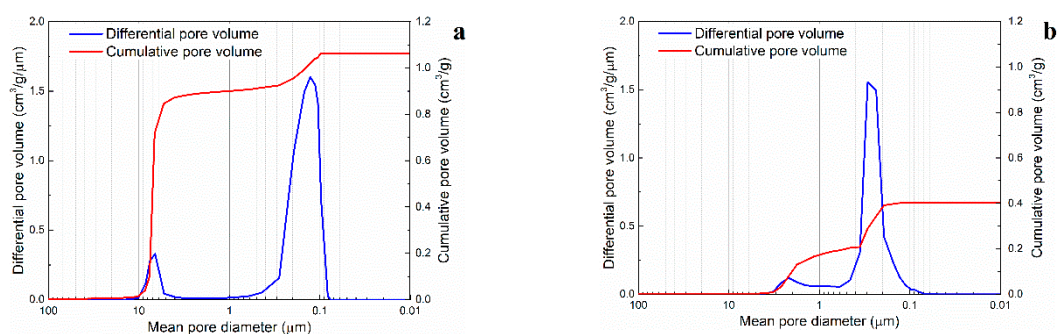


Figure 9. Pore size distribution of presintered alumina foams prepared with WE 20 μm Expancel[®] microspheres, as determined by mercury intrusion porosimetry: (a) 76.0 vol. % porosity and (b) 61.6 vol. % porosity foams.

The alumina foams presintered at 1200 °C exhibited total porosities between 65.7 and 80.2 vol. %, corresponding to compressive strengths of 40.0 ± 3.6 and 7.7 ± 0.5 MPa, respectively (Table 3). These results are comparable to the compressive strength of sintered macroporous alumina foams reported in the literature. According to a study by Han et al. [36], densification and mechanical strength of alumina are optimized after sintering at 1550 °C. Nevertheless, temperatures in the range 1550–1700 °C have been widely used in the processing of macroporous alumina foams. Among others, Gonzenbach et al. [17] produced alumina foams with 88 vol. % porosity and compressive strength of 16 MPa after sintering at 1575 °C. Dhara et al. [37] obtained alumina scaffolds with 71 vol. % porosity and compressive strength of 46 MPa after sintering at 1600 °C. Mao et al. [38] processed macroporous alumina with approximate porosities of 75 and 82 vol. % and approximate compressive strengths of 50 and 20 MPa, respectively, after sintering at 1650 °C. These results are comparable to those obtained in the present study for presintered alumina foams. It is thus suggested that the increase in the sintering temperature could offer macroporous alumina scaffolds with superior mechanical strengths than those already reported in literature.

4. Conclusions

A suitable processing route to produce macroporous alumina scaffolds using wet pre-expanded polymeric microspheres as sacrificial templates has been developed. With this method, the expansion of the microspheres during the process was avoided. The vol. % porosity and the pore size distribution of the alumina foams were tailored with the amount and type of microspheres added to the slurry, respectively. Furthermore, the shape distortion of the microspheres during the preparation of the ceramic slurries was observed to be negligible, which resulted in the shape of the pores being controlled by that of the pre-expanded microspheres. The presintered macroporous alumina foams contained porosity from 65.7 to 80.2 vol. %, with mechanical strengths ranging from 3.3 MPa to 43.6 MPa. The alumina foams exhibited uniform microstructures, with well-dispersed pores and no evident defects. Given the pore size ranges and the degrees of openness achieved, wet pre-expanded polymeric microspheres could be used to produce highly porous ceramic foams with tailored microstructure for filtration, separation, and support for catalysts purposes.

Author Contributions: F.A. and J.N. conceived the idea and planned the research work. M.C.O. performed the experimental work and wrote the draft of the manuscript. All authors contributed in writing to finalize the manuscript.

Funding: This research was funded by Akzo Nobel Pulp and Performance Chemicals AB, Sundsvall, Sweden. Farid Akhtar acknowledges the Infrastructure Fellowship grant RIF14-0083 from Swedish Foundation of Strategic Research.

Acknowledgments: The authors would like to thank Akzo Nobel Pulp and Performance Chemicals AB, Sundsvall, Sweden for providing the polymeric microspheres, as well as all the technical information required for the successful completion of this study.

Conflicts of Interest: The authors declare no conflict of interest.

References

1. Sobsey, M.D.; Stauber, C.E. Point of use household drinking water filtration: A practical, effective solution for providing sustained access to safe drinking water in the developing world. *Environ. Sci. Technol.* **2008**, *42*, 4261–4267. [[CrossRef](#)] [[PubMed](#)]
2. Liang, B.; Zhang, N. Applications of porous SiC ceramics in automobile exhaust purification field. In Proceeding of the International Conference on Electric Information and Control Engineering (ICEICE), Wuhan, China, 15–17 April 2011. [[CrossRef](#)]
3. Gómez-Martín, A.; Orihuela, M.P. Permeability and mechanical integrity of porous biomorphic SiC ceramics for application as hot-gas filters. *Mater. Des.* **2016**, *107*, 450–460. [[CrossRef](#)]
4. Kennedy, M.W.; Zhang, K. Characterization of ceramic foam filters used for liquid metal filtration. *Metall. Mater. Trans. B* **2013**, *44B*, 671–690. [[CrossRef](#)]
5. Wang, Z.; Feng, P. Porous mullite thermal insulators from coal gangue fabricated by a starch-based foam gel-casting method. *J. Aust. Ceram. Soc.* **2017**, *53*, 287–291. [[CrossRef](#)]
6. O'Brien, F.J. Biomaterials & scaffolds for tissue engineering. *Mater. Today* **2011**, *14*, 88–95. [[CrossRef](#)]
7. Hammel, E.; Ighodaro, O.R. Processing and properties of advanced porous ceramics: An application based review. *Ceram. Int.* **2014**, *40*, 15351–15370. [[CrossRef](#)]
8. Mohanta, K.; Kumar, A. Low cost porous alumina with tailored microstructure and thermal conductivity prepared using rice husk and sucrose. *J. Am. Ceram. Soc.* **2014**, *97*, 1708–1719. [[CrossRef](#)]
9. Despois, J.F.; Mortensen, A. Permeability of open-pore microcellular materials. *Acta Mater.* **2005**, *53*, 1381–1388. [[CrossRef](#)]
10. Ashby, M.F.; Mehl Medalist, R.F. The mechanical properties of cellular solids. *Metall. Trans. A* **1983**, *14*, 1755–1769. [[CrossRef](#)]
11. Studart, A.R.; Gonzenbach, U.T. Processing Routes to Macroporous Ceramics: A Review. *J. Am. Ceram. Soc.* **2006**, *89*, 1771–1789. [[CrossRef](#)]
12. Ocampo, J.I.G.; Sierra, D.M.E. Porous bodies of hydroxyapatite produced by a combination of the gel-casting and polymer sponge methods. *J. Adv. Res.* **2016**, *7*, 297–304. [[CrossRef](#)] [[PubMed](#)]
13. Bhaskar, S.; Park, J.G. Thermal and mechanical behavior of ZrTiO₄-TiO₂ porous ceramics by direct foaming. *Ceram. Int.* **2016**, *42*, 14395–14402. [[CrossRef](#)]
14. Barg, S.; Guzi de Moraes, E. New cellular ceramics from high alkane phase emulsified suspensions (HAPES). *J. Eur. Ceram. Soc.* **2009**, *29*, 2439–2446. [[CrossRef](#)]
15. Turnsek, M.; Krajnc, P. Macroporous alumina with cellular interconnected morphology from emulsion templated polymer composite precursors. *J. Eur. Ceram. Soc.* **2016**, *36*, 1045–1051. [[CrossRef](#)]
16. García-Tuñón, E.; Machado, G.C. Complex ceramic architectures by directed assembly of 'responsive' particles. *J. Eur. Ceram. Soc.* **2017**, *37*, 199–211. [[CrossRef](#)]
17. Gonzenbach, U.T.; Studart, A.R. Macroporous Ceramics from Particle-Stabilized Wet Foams. *J. Am. Ceram. Soc.* **2007**, *90*, 16–22. [[CrossRef](#)]
18. Barg, S.; Soltmann, C. Cellular Ceramics by Direct Foaming of Emulsified Ceramic Powder Suspensions. *J. Am. Ceram. Soc.* **2008**, *91*, 2823–2829. [[CrossRef](#)]
19. Liu, R.; Xu, T. A review of fabrication strategies and applications of porous ceramics prepared by freeze-casting method. *Ceram. Int.* **2016**, *42*, 2907–2925. [[CrossRef](#)]
20. Huang, Y.; Yang, J. *Novel Colloidal Forming of Ceramics*; Springer: Berlin/Heidelberg, Germany, 2011; pp. 74–125. ISBN 978-3-642-12281-1.
21. Gilissen, R.; Erauw, J.P. Gelcasting, a near net shape technique. *Mater. Des.* **2000**, *21*, 251–257. [[CrossRef](#)]
22. Tabrizian, P.; Golestanifard, F. The influence of gelcasting parameters on the preparation of Si porous bodies. *Mater. Lett.* **2016**, *183*, 19–22. [[CrossRef](#)]
23. Rao, R.R.; Mariappan, L. Fabrication of micro-featured shapes of alumina ceramics. *Procedia Mater. Sci.* **2014**, *5*, 2595–2604. [[CrossRef](#)]
24. Qian, H.; Cheng, X. Preparation of porous mullite ceramics using fly ash cenosphere as a pore-forming agent by gelcasting process. *Int. J. Appl. Ceram. Technol.* **2014**, *11*, 858–863. [[CrossRef](#)]

25. Dash, S.R.; Sarkar, R. Gel casting of hydroxyapatite with naphthalene as pore former. *Ceram. Int.* **2015**, *41*, 3775–3790. [[CrossRef](#)]
26. Wan, W.; Feng, Y. Preparation of mesoporous silica ceramics with relatively high strength from industrial wastes by low-toxic aqueous gel-casting. *J. Eur. Ceram. Soc.* **2015**, *35*, 2163–2170. [[CrossRef](#)]
27. Andersson, L.; Bergström, L. Gas-filled microspheres as an expandable sacrificial template for direct casting of complex-shaped macroporous ceramics. *J. Eur. Ceram. Soc.* **2008**, *28*, 2815–2821. [[CrossRef](#)]
28. Shin, B.S.; Seul, S.D. Thermal decomposition of copolymers of methyl methacrylate and alkyl methacrylates obtained from a CSTR. *Korean J. Chem. Eng.* **1994**, *11*, 74–80. [[CrossRef](#)]
29. Tong, L.F.; Ma, H.Y. Thermal decomposition and flammability of acrylonitrile-butadiene-styrene/multi-walled carbon nanotubes composites. *Chin. J. Polym. Sci.* **2008**, *26*, 331–339. [[CrossRef](#)]
30. Wicinska, P. Thermal degradation of organic additives used in colloidal shaping of ceramics investigated by the coupled DTA/TG/MS analysis. *J. Therm. Anal. Calorim.* **2016**, *123*, 1419–1430. [[CrossRef](#)]
31. McNeill, I.C.; Sadeghi, S.M.T. Thermal stability and degradation mechanisms of poly(acrylic acid) and its salts: Part 1 poly(acrylic acid). *Polym. Degrad. Stable* **1990**, *29*, 233–246. [[CrossRef](#)]
32. Bednarek, P.; Szafran, M. Thermal decomposition of monosaccharides derivatives applied in ceramic gelcasting process investigated by the coupled DTA/TG/MS analysis. *J. Therm. Anal. Calorim.* **2012**, *109*, 773–782. [[CrossRef](#)]
33. Naranda, J.; Sušec, M. Polyester type polyHIPE scaffolds with an interconnected porous structure for cartilage regeneration. *Sci. Rep.* **2016**, *6*. [[CrossRef](#)] [[PubMed](#)]
34. Guan, B.; Zhan, R. Review of the state-of-the-art of exhaust particulate filter technology in internal combustion engines. *J. Environ. Manag.* **2015**, *154*, 225–258. [[CrossRef](#)] [[PubMed](#)]
35. Pulko, I.; Krajnc, P. High Internal Phase Emulsion Templating—A Path to Hierarchically Porous Functional Polymers. *Macromol. Rapid Commun.* **2012**, *33*, 1731–1746. [[CrossRef](#)] [[PubMed](#)]
36. Han, Y.S.; Li, J.B. The effect of sintering temperatures on alumina foam strength. *Ceram. Int.* **2002**, *28*, 755–759. [[CrossRef](#)]
37. Dhara, S.; Bhargava, P. Influence of Slurry Characteristics on Porosity and Mechanical Properties of Alumina Foams. *Int. J. Appl. Ceram. Technol.* **2006**, *3*, 382–392. [[CrossRef](#)]
38. Mao, X.; Shimai, S. Gelcasting of alumina foams consolidated by epoxy resin. *J. Eur. Ceram. Soc.* **2008**, *28*, 217–222. [[CrossRef](#)]



© 2018 by the authors. Licensee MDPI, Basel, Switzerland. This article is an open access article distributed under the terms and conditions of the Creative Commons Attribution (CC BY) license (<http://creativecommons.org/licenses/by/4.0/>).